

## **Diagnostics of relativistic runaway electrons in a tokamak plasma based on laser inverse Compton scattering**

Y. Kawano, T. Kondoh, T. Hatae

*Japan Atomic Energy Agency, Naka, Ibaraki, 311-0193 Japan*

### **1. Introduction**

During a major disruption of a discharge in ITER, a high-current runaway electron beam can be formed. Since serious damages of plasma facing components are expected when intense and localized bombardment of the runaway electrons occurs, development of techniques for mitigating the negative influences caused by the runaway electrons is very important subject. Here, in order to understand the dynamics of the runaway electron beam in the plasma, we have proposed an active diagnostic method based on the laser inverse Compton scattering (LCS) [1~3]. In this paper, improved discussions on the energy spectra of LCS photons, background radiations, and the signal to noise ratio are presented.

### **2. Energy spectra of LCS photons**

In JT-60U, energy of post-disruption runaway electrons is estimated to be as high as  $E_e \sim 30$  MeV [4], where  $E_e$  is electron energy. The LCS photon energy  $E_s$  shows its maximum value in the case of  $\alpha=0^\circ$  and  $\theta=180^\circ$ , where  $\alpha$  is the collision angle between a relativistic electron and an incident photon (head-on collision),  $\theta$  is the scattering angle between the electron and a scattered photon (forward scattering). The maximum value of  $E_s$  is obtained in such geometry as  $E_s^{\max}=4\gamma^2 E_i$ , where  $\gamma$  is the relativistic Lorenz factor. For instance,  $E_s^{\max}$  will be  $\sim 16$  keV for an incident YAG<sup>1st</sup> laser photon ( $\lambda=1.06$   $\mu\text{m}$ ,  $E_i=1.17$  eV) with  $E_e \sim 30$  MeV ( $\gamma \sim 60$ ). It is presumably expected that beam electrons have distribution in their energy, and this is what we pursue. Spectra of LCS photons should be modified from those of ordinary LCS spectra for mono-energy in  $E_e$  due to contributions from every energy components of electrons. For evaluation of this effect, test functions of energy spectrum of runaway electrons are prepared as shown in Fig.1, i.e. (a) a flat shape in  $E_e$ , (b) negative e-folding shape;  $\exp\{-5(E_e/50)\}$ , and (c) positive e-folding shape;  $\exp\{5(E_e/50)\}$  ( $E_e$  in MeV). Total numbers of beam electrons for  $E_e = 1 \sim 50$  MeV are same in Fig.1 (a), (b) and (c)). Figure 2 shows obtained LCS spectra corresponding to the test functions in Fig.1. Since the difference is obviously recognized between shapes of those

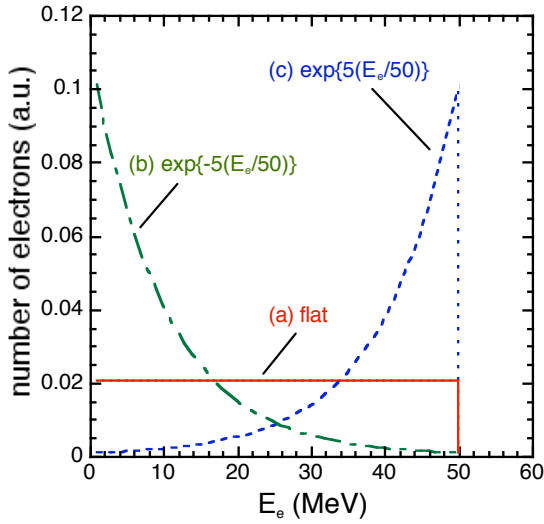


Fig. 1 Test functions of energy spectrum of runaway electrons

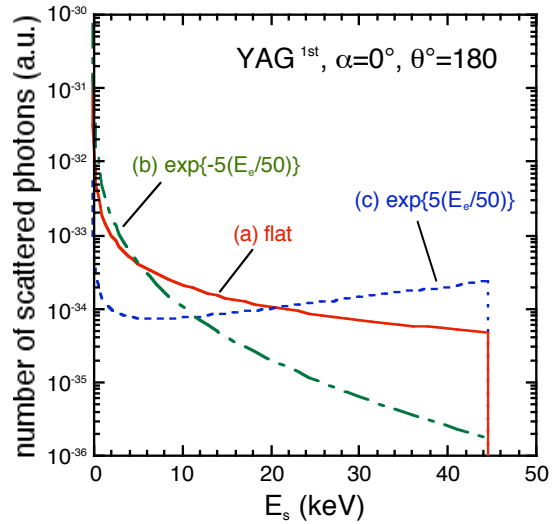


Fig. 2 LCS spectra corresponding to the test functions in Fig.1

LCS spectra, we expect that the energy distribution of the runaway electrons can be evaluated from measured LCS spectra.

### 3. Background radiations

Natural or background radiation processes in a tokamak plasma under the presence of runaway electrons are investigated. Background radiations are important not only for evaluation of noise components in the LCS concept but also for diagnostic of runaway electrons by themselves. Those processes include the relativistic bremsstrahlung radiation, the synchrotron radiation, and the inverse Compton scattering. We basically adopt expressions in Langair [5,6] for the energy loss rate of a relativistic electron  $-dE_e/dt$  and the maximum energy of radiation spectra  $E_{hv}^{max}$ . Example plasma parameters of a post-disruption runaway plasma observed in JT-60U are as follows [4]; bulk electron temperature  $T_e=10$  eV, bulk electron density  $n_e=2 \times 10^{19} \text{ m}^{-3}$ , atomic number  $Z=10$  (neon), ionic charge  $Z_i=3$ , beam electron density  $n_b=1 \times 10^{15} \text{ m}^{-3}$ , and toroidal magnetic field  $B_t=3.73$  T. (1) Relativistic bremsstrahlung radiation: to discuss partially ionized atoms in a post-disruption runaway plasma, we simply take a sum of  $-dE_e/dt$  for neutral atoms by Bethe-Heitler and  $-dE_e/dt$  for ions with the Debye shielding length as a collision parameter. (2) Synchrotron radiation: pitch angle of an electron is scanned from  $0.36^\circ$  (which corresponds to perpendicular electron temperature of 10 eV) to  $90^\circ$ . (3) Inverse Compton scattering: considered radiation fields are blackbody radiation in the vacuum vessel which temperature is 573 K, thermal bremsstrahlung radiation for above shown plasma parameters, and  $H_\alpha$  radiation. For latter two cases, we define the confinement (or persistence) time of

photon as  $L/c$ , where  $L$  is the scale length of the confinement volume of photons ( $L \sim 1.5$  m for JT-60U) and  $c$  is the speed of light.

Figures 3 and 4 show  $-dE_e/dt$  and  $E_{\text{hv}}^{\text{max}}$  for  $E_e = 1$  MeV  $\sim$  50 MeV and Table 1 summarise them (line numbers in Figs. 3 and 4 correspond to those in Table 1). Thus, we identified possible ranges of  $-dE_e/dt$  and  $E_{\text{hv}}^{\text{max}}$  for a post-disruption runaway plasma in JT-60U.

#### 4. Signal to noise ratio

From results of the previous section, we aware that synchrotron radiation can exhibit a large  $-dE_e/dt$ . On the other hand, its  $E_{\text{hv}}^{\text{max}}$  is in VUV region. Therefore, synchrotron radiation does not contaminate the measurement of LCS photons in X-rays. The  $E_{\text{hv}}^{\text{max}}$  for relativistic bremsstrahlung and inverse Compton scattering is in  $\gamma$ -rays and hard X-rays regions, respectively. However,  $-dE_e/dt$  of inverse Compton scattering is extremely low. Therefore, we confirm that relativistic bremsstrahlung is the major background radiation for noise component.

The number of LCS photons towards a detection area of 0.2 m x 0.2 m located at 4 m from the interaction volume at the plasma center will be  $\sim 6000$  in the case of that the LCS geometry and conditions in JT-60U are as follows;  $E_e = 30$  MeV, incident laser is YAG<sup>1st</sup> (laser power=10 J, pulse length=1 ns),  $\alpha = 0^\circ$ ,  $\theta = 180^\circ$ , and plasma parameters are same as those shown in the previous section [3]. The  $E_s$  at the detection area is distributed from 5.4 keV to 16 keV due to  $\theta$  dependence of  $E_s$ . In this case, number of photons of the relativistic bremsstrahlung for the energy width of  $\sim 10$  keV will be up to  $\sim 1900$ . Therefore, the signal to noise ratio  $S/N$  is estimated as  $\sim 3$ . This number provides a base to design the instruments in the actual tokamak device.

#### 5. Discussions

As shown in section 3, there are various background radiation processes in a post-disruption runaway plasma. Naturally, simultaneous measurements of LCS and background radiations are useful for diagnostics of runaway electrons.

Apart from the diagnostics, any kind of radiations is closely coupled to the behavior of runaway electrons via energy loss and momentum change by radiations. Therefore, we propose a new subject for active control of runaway electrons under the viewpoint of control of radiations by external means.

This work was supported by the Grant-in-Aid for Scientific Research from Ministry of Education, Culture, Sports and Technology (No. 16204049).

- [1] Y. Kawano et al., Proc. Plasma Science Symposium 2005 / The 22<sup>nd</sup> Symposium on Plasma Processing, 26-28 January 2005, Will Aichi, Nagoya, Japan (2005) 93-94.
- [2] Y. Kawano et. al, for the papers of Technical Meeting on Pulsed Power Technology, IEE Japan, 6 Feb. 2006, Wajima, Japan, PPT-06-18 (2006) 95-98.
- [3] The Institute of Electrical Engineers of Japan, Technical Report No. 1018 (2005) 25-29 (in Japanese).
- [4] Y. Kawano et al., J. Plasma Fusion Research **81** (2005) 593-601.
- [5] M. Longair, High Energy Astrophysics 2nd Ed. Vol.1 (Cambridge Univ. Press, 2004).
- [6] M. Longair, High Energy Astrophysics 2nd Ed. Vol.2 (Cambridge Univ. Press, 2002).

Table 1 Summary of evaluation of background radiations

No.	Radiation Process	Parameters and conditions	$-dE_e/dt$ (J/s) @ $E_e=30\text{MeV}$	$E_{h\nu}^{\max}$ (eV) @ $E_e=30\text{MeV}$
1	Relativistic Bremsstrahlung	$n_e=2\times 10^{19}\text{m}^{-3}$ , $T_e=10\text{eV}$ , $Z=10$ , $Z_i=3$	$1.4\times 10^{-12}$	$3\times 10^7$
2	Synchrotron	$B=3.73\text{T}$ , pitch=90deg	$7.6\times 10^{-10}$	9.3
3	Synchrotron	$B=3.73\text{T}$ , pitch=45deg	$3.8\times 10^{-10}$	6.6
4	Synchrotron	$B=3.73\text{T}$ , pitch=3.6deg	$3\times 10^{-12}$	0.6
5	Synchrotron	$B=3.73\text{T}$ , pitch=0.36deg	$3\times 10^{-14}$	0.06
6	Inverse Compton	Black Body 573K	$8\times 10^{-21}$	$3.4\times 10^3$
7	Inverse Compton	Thermal Brems $T_e=10\text{eV}$	$4\times 10^{-23}$	$2.8\times 10^5$
8	Inverse Compton	$H\alpha$	$4\times 10^{-25}$	$2.6\times 10^4$

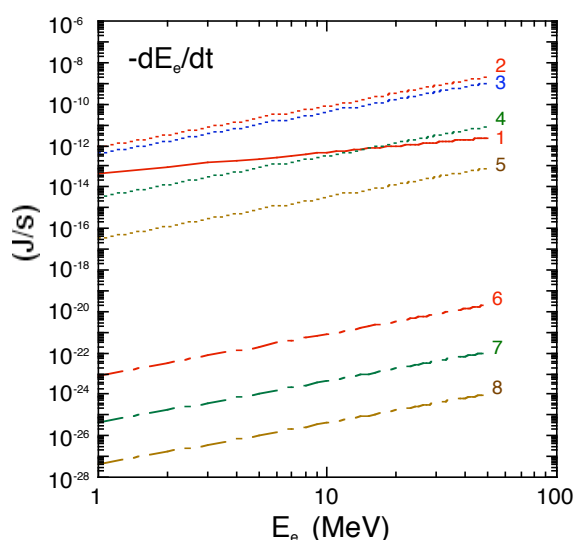


Fig. 3 Energy loss rate of relativistic electrons  $-dE_e/dt$  as a function of electron energy  $E_e$ . Line numbers are correspond to those in Table 1.

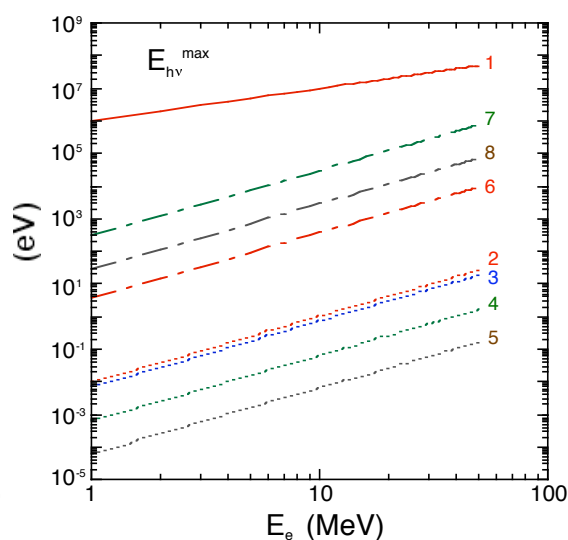


Fig. 4 Maximum energy of radiation spectra  $E_{h\nu}^{\max}$  as a function of electron energy  $E_e$ . Line numbers are correspond to those in Table 1.